

Equilibrium segregation of Ti to Au–sapphire interfaces

Elad Nussbaum · Hila Meltzman · Wayne D. Kaplan

Received: 10 May 2011 / Accepted: 9 June 2011 / Published online: 28 June 2011
© Springer Science+Business Media, LLC 2011

Abstract Equilibrium segregation of Ti to Au–sapphire interfaces was measured from dewetted Au(Ti) films on the (0001) surface of sapphire. Quantitative energy dispersive spectroscopy was used to determine a Ti excess at the Au–sapphire interface of 2.2 Ti atoms/nm², which together with an excess of 4.6 Ti atoms/nm² at the (0001) sapphire surface, is associated with a decrease in the solid–solid Au–sapphire interface energy. Quantitative high resolution transmission electron microscopy showed that the segregated Ti is distributed within a 1.54-nm thick intergranular film at the Au–sapphire interface, which is not a bulk phase but rather an equilibrium interface state. As a result, Ti segregation without the formation of a bulk reaction at the interface is associated with a decreased interface energy, improved wetting, and may be an important part of the total complex mechanism responsible for improved wetting and spreading in “reactive” braze systems.

Introduction

Alloying elements (dopants) are often added to solders and brazes to promote spreading and adhesion, in particular, for joining ceramic oxides [1–3]. This is done for a number of reasons related to both the process of joining (dependent upon the kinetics of spreading) and the subsequent adhesion of the solid–solid metal–ceramic interface (which is defined by solid–solid wetting). On one hand, the wetting of liquid metals on ceramics (and oxides in particular) is poor, reflected by relatively high contact angles when

determined from sessile drop experiments. High contact angles reflect the relatively high solid–liquid interface energy, and can result in the formation of pores at the interfaces of joins [4, 5], and detrimentally affect the rate of spreading of the liquid during the joining process [6]. After solidification of the solder/braze alloy, the solid–solid metal–ceramic interface energy is a critical component of the thermodynamic work of adhesion of the interface, which is the basis for mechanical adhesion [7].

While alloying can be used to engineer the properties of bulk braze alloys, for wetting, spreading, and adhesion it is the nature of the metal–ceramic interface which is critical. Different techniques have been developed for improving metal–ceramic joining processes. In some cases, the ceramic can be modified to improve wetting and spreading [8], but one of the most common approaches is the so called active joining or active metal brazing process, where the braze metal is alloyed with small amounts of wetting promoters; metals such as Ti, Zr, V, Cr, and Hf. These metals induce a change in the chemistry and/or structure of the metal–ceramic interface, resulting in a reduction of the solid–liquid interfacial energy and presumably a decrease in the solid–solid metal–ceramic interfacial energy after solidification of the braze alloy. The wetting or spreading in such systems is usually referred to as Reactive wetting/spreading, although whether a reaction at the interface is required to reduce the interface energy is under debate.

Numerous results can be found in the literature about improved wetting via the addition of active elements, with Ti being one of the most studied [9]. For example, Kapoor et al. [10] reported that alloying Ag with 2 at% Ti resulted in a decrease of the liquid contact angle from 135° to 40–45° on polycrystalline Al₂O₃. Kritsalis et al. showed that alloying Cu with Ti improves its wetting on Al₂O₃ [11, 12]. Gremillard et al. [13] found that additions of

E. Nussbaum · H. Meltzman · W. D. Kaplan (✉)
Department of Materials Engineering, Technion—Israel Institute
of Technology, Haifa 32000, Israel
e-mail: kaplan@tx.technion.ac.il

1 wt% Ti to a Sn–3 wt% Ag alloy decreased the contact angle on sapphire ($\alpha\text{-Al}_2\text{O}_3$) from 150° to 25° . Similar results were reported for braze alloys on nitrides, carbides, and carbon [14–17].

While there is no doubt that “active elements” affect wetting and spreading of metals on ceramics, there is an ongoing argument about the exact mechanism and related thermodynamic phenomena taking place at the metal–ceramic interface. In addition to the important influence of capillary driven triple-line morphological changes on spreading [18–21], equilibrium segregation (Gibbsian segregation) and/or interface reactions can influence wetting, and thus spreading [22]. Gibbsian segregation can be defined as the reduction of interface energy due an excess of solute at the interface. This is identical to adsorption (which is usually termed to describe a surface excess originating from the gas phase), and does not involve the formation of a new bulk phase at the interface (i.e., no bulk chemical reaction takes place). Since the interfacial excess associated with equilibrium segregation can be at sub-monolayer levels, there is relatively limited data in the literature indicating that this mechanism is dominant in braze alloys [23, 24]. On the other hand, a relatively large number of studies experimentally confirmed the existence of interfacial reaction products by scanning electron microscopy (SEM) due to the addition of active elements [2, 25–37]. Under these conditions, wetting is now defined via the interfacial energy between the liquid braze alloy and the reaction products at the interface (or on the surface of the substrate).

In the following an experimental approach is described which can be used to elucidate the mechanism responsible for improved adhesion due to active elements. The approach is based on wetting (rather than the kinetics of spreading) to address equilibrium segregation, and utilizes the equilibrated state of a dewetted metal film on a solid substrate. In the system studied here, the interface state of solid Au equilibrated in contact with the basal (0001) plane of sapphire is characterized in the presence of Ti.

Experimental methods

Sample preparation

The hypothesis here is that Ti segregates to the interface between metals and alumina, and thus reduces the interface energy. To prove this, a model system is required where several conditions are met:

1. Ti is available as a solute, below the solubility limit, in either the metal or the substrate, but preferably not located at the interface before equilibration;

2. The solid–solid interface energy can be evaluated, since this parameter defines the thermodynamic work of adhesion of the solidified join;

3. The same interface used to determine the interface thermodynamics can be characterized regarding its structure and chemistry.

4. The partial pressure of oxygen must be known, since this is a critical thermodynamic parameter of the system.

To reach these conditions, a model system was used based on thin continuous Au films, doped with Ti, which were deposited on the (0001) surface of sapphire by RF magnetron sputtering. The Au was doped with Ti via an intermediate Ti layer which was deposited at a defined distance from the interface with the sapphire substrate. During thermal equilibration, the continuous Au film broke-up (dewetted) into small particles, driven by the minimization of surface and interface energy of the system.

Sapphire substrates of 99.99% purity (supplied by Gavish Industrial Technologies and Materials LTD, Omer Israel) with a basal (0001) orientation were used for the dewetting experiments. Polished substrates were ultrasonically cleaned in acetone and ethanol, followed by annealing in air at 1200°C for 2 h. A layered coating was deposited on the sapphire substrates by RF magnetron sputtering at a base pressure of 5.4 mtorr Ar, while the substrates were maintained at 200°C . The thickness of layers 1 and 3 (see Fig. 1) corresponding to the Au was 204 nm each, and the thickness of the Ti layer (layer 2) was 8 nm. The layer thickness was confirmed from cross-section transmission electron microscopy (TEM). This layer thickness gave a total Ti concentration of 1.86 at% (0.46 wt%), which is below the solubility limit for both the liquid and solid state of Au. The Ti layer was deposited between the two Au layers without breaking vacuum to avoid exposing it to oxygen in ambient air, thus preventing it from oxidizing.

Samples were then annealed within a sapphire tube located in a quartz tube furnace under a constant flow of pure Ar (99.999%) at a pressure slightly above the ambient. The sapphire tube was used to prevent contamination from the quartz tube [38]. Before entering the sapphire tube in the furnace, the Ar was passed through an oxygen getter containing Ti and Cu flakes heated to 900°C . This reduced the partial pressure of oxygen to $\sim 10^{-21}$ atm.

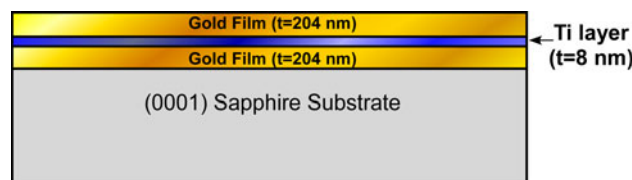


Fig. 1 Schematic drawing of the as-deposited Au films on the basal (0001) surface of sapphire, with a thin film of Ti

The dewetting thermal equilibration profile was as follows (see Fig. 2): The as-deposited films were heated to 1100 °C (at 10 °C/min) to melt the Au(Ti) film. This temperature was selected from the Au–Ti phase diagram to ensure liquid-state dewetting [39]. Due to a relatively high contact angle of liquid Au on sapphire, liquid-state dewetting will rapidly occur [40, 41]. After holding for 6 min at 1100 °C, the samples were cooled to 700 °C (at 15 °C/min) to ensure solidification of the dewetted droplets. Cooling to 700 °C was followed by heating to 900 °C (at 10 °C/min) where the sample was annealed for 1 h, under constant gas flow, and then cooled to ambient. This dewetting experiment resulted in the creation of a very large number of partially faceted particles with diameters ranging from few hundreds of nanometers to several microns (see Fig. 3).

The equilibration time (τ), for a spherical particle with radius r can be estimated from [42, 43]:

$$\tau = \frac{r^4 kT}{24\gamma D_s \nu \Omega^2} \quad (1)$$

where k is Boltzmann’s constant (3.38065×10^{-23} J/K), T is the absolute temperature of the equilibration experiment (1173 K), γ is the surface energy (1.4 J/m² [44]), D_s is the surface diffusivity (5×10^{-10} m²/s [42]), ν is the number of atoms per unit surface area (1.2×10^{19} m⁻²) and Ω is the atomic volume (1.7×10^{-29} m³). Using Eq. 1, particles with radius of 1 μ m will equilibrate in just under 5 min (4.6 min) at 900 °C.

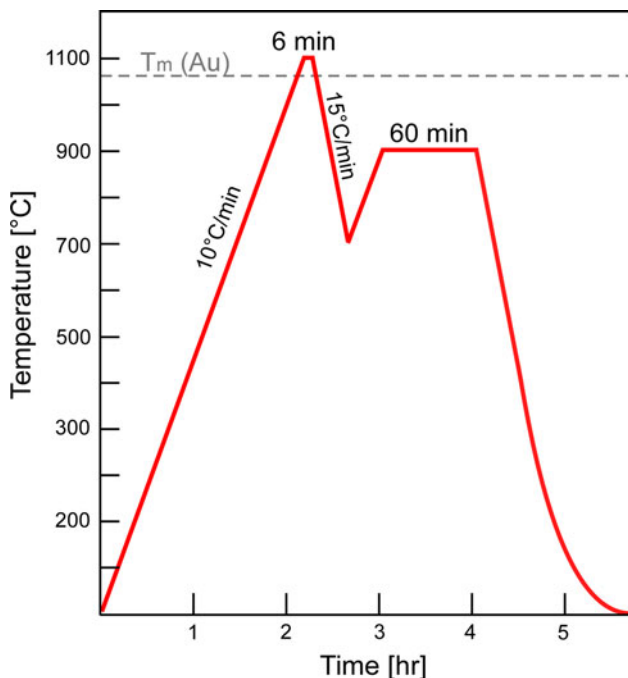


Fig. 2 Schematic drawing of the annealing cycle used to dewet and equilibrate the Au films

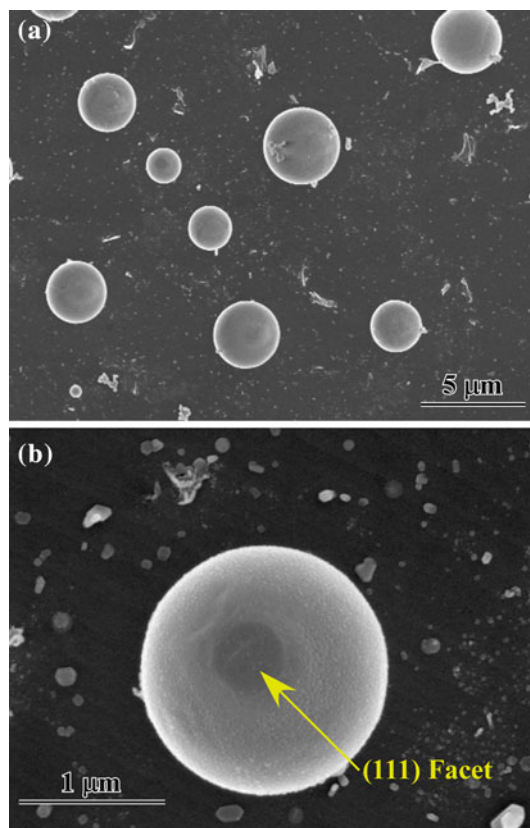


Fig. 3 Secondary electron SEM micrographs of the **a** dewetted Au film and **b** a single Au particle with a visible facet (arrowed). The micrographs were recorded after applying a thin Cr conductive coating to prevent charging under the electron beam, which is visible in the form of fine contrast on the surface of the particle. The debris on the sapphire substrate are alumina particles which were inadvertently introduced after equilibration and before microscopy

Characterization

Preferred orientation of the Au particles on the sapphire substrate was examined by X-ray diffraction (XRD), using a conventional X-ray diffractometer (Philips X’pert goniometer) with CuK α radiation operated at 40 kV and 40 mA. A θ – 2θ scan was conducted from 35° to 145°, with a step size of 0.04° and an exposure time of 8 s for each step.

The morphology and shape of the dewetted particles were examined by SEM and high resolution SEM (HRSEM). SEM examination was conducted using an FEI Quanta 200 SEM, using varying accelerating voltages (5–20 kV) and a working distance of 10 mm. The SEM was equipped with energy and wavelength dispersive spectrometers (EDS/WDS, Oxford Instruments) for chemical analysis. HRSEM was conducted on a FEI Strata 400 s dual beam focused ion beam (FIB) system, equipped with a field emission gun SEM. An accelerating voltage of 5 kV and a working distance of 5 mm were used for HRSEM.

Characterization of the metal–ceramic interface was conducted using TEM. Cross-section specimens for TEM were prepared from selected particles using the FIB and the “in-situ lift-out” technique. The initial lamella thickness was ~ 0.2 – 0.3 μm . Further low voltage polishing (2–5 kV) was used to thin the lamella to less than 100 nm [45, 46]. Confirmation of the as-deposited layer thickness was done using an FEI Tecnai G2 T20 S-Twin S/TEM at 200 kV. High resolution TEM (HRTEM) of the metal–ceramic interface was done using a monochromated and (image) aberration corrected FEI Titan at 300 kV. Quantitative HRTEM analysis was based on retrieval of the complex electron wave function at the exit surface of the specimen using electron holography. In this method, the wave function is reconstructed from a series of experimental micrographs recorded as a function of objective lens defocus [47]. By reconstructing the exit wave, imaging artifacts are removed, especially residual delocalized contrast. Exit wave reconstruction of the defocus series was conducted using True Image (FEI). To confirm the solution of the exit wave function, the reconstructed exit wave was compared to the reconstructed exit wave from a simulated defocus series calculated using the EMS software package [48]. Iterative digital image matching (IDIM) was used to determine the objective lens defocus of specific images from the series [49].

Elemental analysis of the interface region was conducted on the Titan using scanning TEM (STEM) mode and EDS (EDAX). Experimental values of the Au–Ti k -factor for quantitative EDS analysis were determined from standards. Standards were prepared from appropriate amounts of Ti and Au to form stoichiometric intermetallic phases using an arc furnace (melted five times under 99.999% Ar). After arc-melting, the sample was sectioned (to expose the bulk) and heat treated at 1000 °C for 70 min at a vacuum level of 1×10^{-5} torr. After heat treatment, the sample was characterized by XRD, SEM–EDS, and SEM–WDS to identify the stoichiometric Au_2Ti intermetallic phase, which was used as a standard. TEM samples of the standard were prepared using the FIB “lift-out” technique as described above. EDS spectra were acquired from the standard as a function of sample thickness to determine absorption independent values of the k -factor [50], which was determined to be $k_{\text{Au–Ti}} = 0.94 \pm 0.18$. The absolute thickness of the interface region was determined using fully calibrated plasmon mean-free-paths and electron energy loss spectroscopy (EELS) [51].

Results

Figure 3 presents HRSEM micrographs of the dewetted particles. Round particles with detectable facets were

observed. It should be noted that the particles are significantly less faceted than those studied previously for gold on sapphire [44], probably due to surface contamination in the previous study leading to a more anisotropic crystal shape (as discussed in [44]). From SEM no specific orientation relationship of the faceted particles with respect to the substrate was visible. This was confirmed from XRD, which showed only a preferred orientation of the (111) Au planes parallel to the (0001) sapphire substrate (Table 1). This result is very different from past studies of pure equilibrated Au particle on the basal plane of sapphire, where two specific low energy orientation relationships were discerned [44, 52].

Figure 4 presents a bright field TEM micrograph and selected area diffraction pattern of a cross section of a Au particle which was identified to have a low-index orientation relationship with the sapphire ($[\bar{1}2\bar{1}0](000\bar{6})_{\text{Al}_2\text{O}_3} \parallel [110](\bar{1}\bar{1}\bar{1})_{\text{Au}}$). While this orientation relationship agrees with previous works [44], this was the single example of a low-index orientation relationship found in the present samples, and thus the preferred orientation found by XRD analysis rather than a specific low-index orientation relationship describes the orientation of the Au particles with respect to the sapphire substrate.

EDS spectra from the interface region were acquired in STEM mode using the Titan while scanning the focused electron probe over a region approximately 125×10 nm. In order to determine the possible excess of Ti at the Au–sapphire interface, a series of EDS scans were conducted at three locations in the sample: (1) in the bulk of the Au particle; (2) at the Au–sapphire interface; and (3) in the bulk sapphire. All three scans were conducted under the same conditions. Ti was not detected in the bulk sapphire. The amounts of Ti in the bulk Au particle and at the Au–sapphire interface were determined following Keast and Williams [53] and the experimentally determined k -factor. The excess of Ti was then obtained by subtracting the amount of Ti in the bulk Au particle from that at the interface, resulting in an excess of 2.2 Ti atoms/ nm^2 at a measured detection limit of 1.8 atoms/ nm^2 (which is three times the background level). Assuming that Ti acts as a substitution atom for Au at the (111) terminating plane at the interface, and based on the atomic density of the Au (111) plane (12 atoms/ nm^2), then 0.18 monolayers of Ti exist as excess at the interface. Assuming that Ti replaces an Al cation at the Al-terminated sapphire interface, and based on a cation density of the c(0001) sapphire surface (10 cations/ nm^2), then there is 0.22 monolayers of Ti excess at the interface. These results are the total interface Ti excess projected onto one crystallographic plane. From this analytical approach, it is not possible to determine the distribution of Ti atoms in a direction normal to the

Table 1 Measured XRD integrated intensities of the dewetted Au film (without reflections from the substrate), together with the simulated intensities for a randomly oriented Au sample

Reflection (<i>hkl</i>)	2θ (°)	Measured intensity <i>I</i> (<i>hkl</i>)	Simulated intensity <i>I'</i> (<i>hkl</i>)	$P = \frac{I_{(hkl)}}{\sum I_{(hkl)}} \cdot \frac{\sum I'_{(hkl)}}{I'_{(hkl)}}$
Au (111)	38.36	100.0	100	1.41
Au (200)	44.56	24.1	52	0.65
Au (220)	64.76	13.8	32	0.61
Au (311)	77.76	18.2	36	0.71

P for (111) is significantly above 1.0, indicating a preferred orientation of this plane parallel to the substrate surface

Bold represents important data indicating a preferred orientation

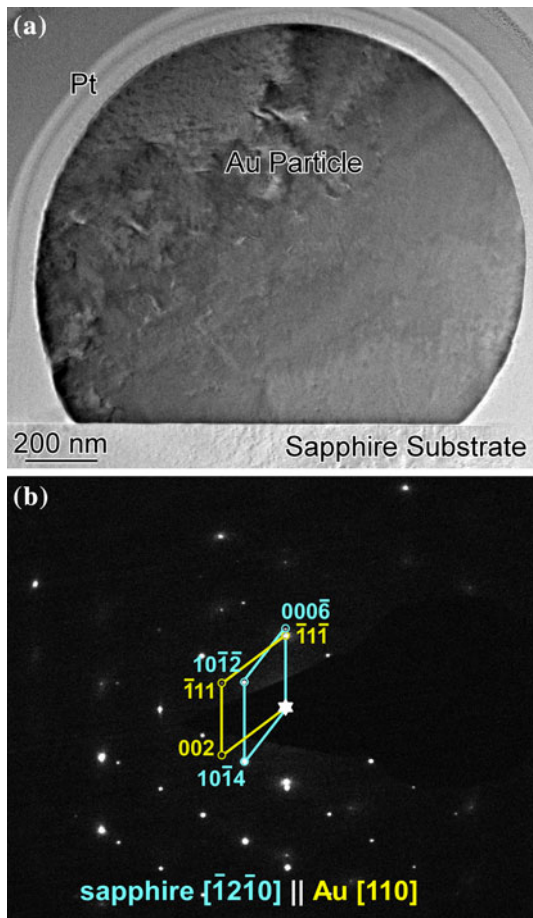


Fig. 4 **a** Bright field TEM micrograph of a cross section of a Au particle on the (0001) sapphire substrate. The selected area diffraction pattern in **b** shows the orientation relationship between the particle and the substrate. The sapphire was oriented in a $[\bar{1}2\bar{1}0]$ zone axis using Kikuchi diffraction before acquiring the selected area diffraction pattern. The Au is in a $[110]$ zone axis, resulting in an orientation relationship of $[\bar{1}2\bar{1}0](000\bar{6})_{\text{Al}_2\text{O}_3} || [110](\bar{1}\bar{1}\bar{1})_{\text{Au}}$

interface. This question is addressed below using quantitative HRTEM.

No Ti was detected as an excess at the surface of the Au particles, and this result is expected since Ti has a higher surface energy than pure Au ($\gamma_{\text{Ti}} = 1.938 \text{ J/m}^2$) [54]. EDS

analysis was conducted at the sapphire surface immediately adjacent to the particles, and following the method outlined above a Ti excess of 4.6 Ti atoms/nm² (corresponding to 0.5 monolayers of Ti excess) was measured, indicating that Ti adsorbs to the (0001) surface of sapphire in addition to the Au–sapphire interface.

Cs-corrected HRTEM micrographs of the same interfaces were acquired, and a single micrograph recorded at approximately 19 nm (positive) focus is presented in Fig. 5. This micrograph was recorded after orienting the sapphire into a $[\bar{1}2\bar{1}0]$ zone axis, ensuring that the (0001) sapphire surface is parallel to the incident electron beam. The Au particle does not have a low-index orientation relationship with the sapphire, so it was not possible to orient both the Au and sapphire in low-index zone axes with the interface parallel to the incident electron beam. The value of objective lens focus was determined using an automated matching procedure to compare the experimental micrograph with simulated images as a function of objective lens focus and thickness. From this raw data, the existence of a $\sim 1.1 \text{ nm}$ thick interface film is evident. The film, which is associated with the measured Ti excess of 2.2 Ti atoms/nm², appears to be partially ordered. However, such a conclusion cannot be reached without taking into account the contribution of contrast delocalization. The maximum value of contrast delocalization can be estimated from [55]:

$$R(g) = Z\lambda g + C_s\lambda^3 g^3 \tag{2}$$

where *Z* is the objective lens focus value (19 nm), λ is the wavelength of the incident electrons (0.00197 nm), *g* is the information limit of the microscope ($g_{\text{max}} = 14.3 \text{ nm}^{-1}$), and *C_s* is the spherical aberration coefficient used to record the micrograph ($-1.7 \mu\text{m}$). At this value of objective lens focus, the maximum contrast delocalization is 0.497 nm, which is approximately half the apparent thickness of the film, and any conclusions regarding the ordered nature of this region could be in error.

To address this point, and to provide a more accurate measure of the film thickness, the exit wave was reconstructed from a series of micrographs acquired as a

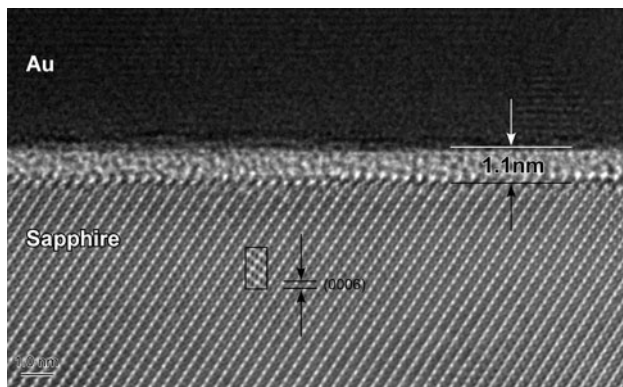


Fig. 5 HRTEM micrograph of the interface region between a Au particle and the sapphire substrate. The sapphire is oriented in a [1210] zone axis. The micrograph was acquired using a Cs of $-1.7 \mu\text{m}$ at a focus of 19 nm. A simulated image for these acquisition parameters is presented in the inset

function of objective lens defocus. The phase of the reconstructed wave is presented in Fig. 6. The positions of the ions in the sapphire substrate were determined by comparing the reconstructed phase with simulated wave functions, which underwent the same reconstruction procedure as that used for the experimental data. From the reconstructed phase it is obvious that the film is actually thicker than that determined from the raw HRTEM data, and that the regions immediately adjacent to the sapphire are strongly ordered. The degree of order appears to decay as a function of distance into the film.

The value of the Au–sapphire interface energy was determined using Winterbottom’s analysis from cross-section TEM micrographs [56], in a way similar to that used in [44]. This approach was used for the solid–solid interface energy, since dihedral analysis at the triple junction could intersect facets and thus would not take into account torque terms [57, 58]. Using Winterbottom’s analysis, reported values of $\gamma_{\text{Au}(111)} = 1.4 \text{ J/m}^2$ [59] and the surface energy of clean (0001) sapphire

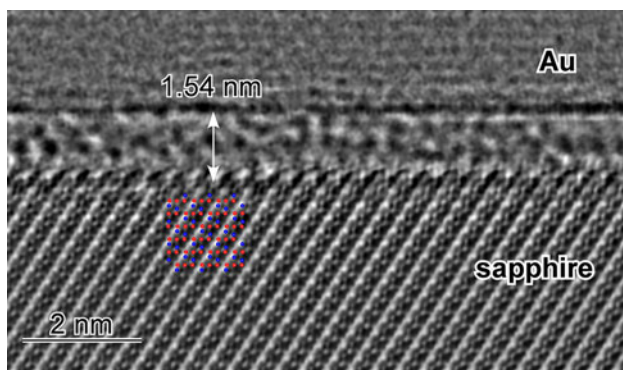


Fig. 6 Phase of the reconstructed electron wave. The atom positions are indicated in the sapphire using *blue circles* for Al cations and *red circles* for oxygen anions (Color figure online)

($\gamma_{\text{S}} = 1.24 \text{ J/m}^2$) [60], the solid–solid substrate–particle interface energy was determined to be $\gamma_{\text{SP}} = 2.02 \pm 0.05 \text{ J/m}^2$ and the thermodynamic work of adhesion $W_{\text{ad}} = 0.62 \pm 0.05 \text{ J/m}^2$.

Discussion

The absolute value of the interface energy measured here ($2.02 \pm 0.05 \text{ J/m}^2$) is approximately equivalent to that measured in the past for the Au–sapphire interface ($\gamma_{\text{SP}} = 2.15 \pm 0.04 \text{ J/m}^2$) [44]. However, the surface energy of the basal plane of sapphire used to determine the interface energy is that of clean sapphire. Here, we have experimentally determined an excess of 4.6 Ti atoms/ nm^2 at the sapphire free surface. Adsorption of Ti to the sapphire free surface is not surprising, and necessarily means that the sapphire surface energy is lower than that of the pure sapphire surface. As such, the realistic value of the Au–sapphire energy from the present experiments should be significantly lower than $2.02 \pm 0.05 \text{ J/m}^2$, due to the measured Ti interface excess. Unfortunately, to the best of our knowledge, the behavior of the surface energy of sapphire as a function of Ti adsorption is not known. Estimating a decrease of 10–20% for the sapphire surface energy due to Ti adsorption, values of 1.116 and 0.992 J/m^2 can be used for γ_{SV} (solid–vapor surface energy), respectively. Substituting these values in the Winterbottom formulation results in a Au–sapphire interface energy in the range of $1.77 < \gamma_{\text{SP}} < 1.90 \text{ J/m}^2$. These values represent a significant decrease in interface energy (compared to [44]).

The influence of Ti segregation to the Au–sapphire interface is also seen by the change in interface anisotropy. The XRD data indicate that the Au (111) plane is the sole preferred orientation ($P > 1$) of the Au particles on (0001) sapphire in the presence of a Ti excess (Table 1). This result is significantly different from the data reported by Fecht and Gleiter [52], and Sadan and Kaplan [44], who found two preferred orientations of pure Au particles equilibrated on (0001) sapphire substrates, Au(111) and Au(200), with defined low-index orientation relationships [44]. The loss of the Au(200) preferred orientation and the change from low-index orientation relationships to a single preferred Au(111) orientation indicates that the Ti excess anisotropically decreases the Au(111)–sapphire interface energy. This can be represented graphically via a schematic γ -plot for pure gold in contact with (0001) sapphire compared to Au doped with Ti (see Fig. 7), where for pure Au there would be two cusps in the interface energy, while Ti segregation deepens the Au(111) cusp.

The combination of quantitative HRTEM analysis together with the analytical measure of Ti excess shows that the Ti segregation is not a simple distribution of excess

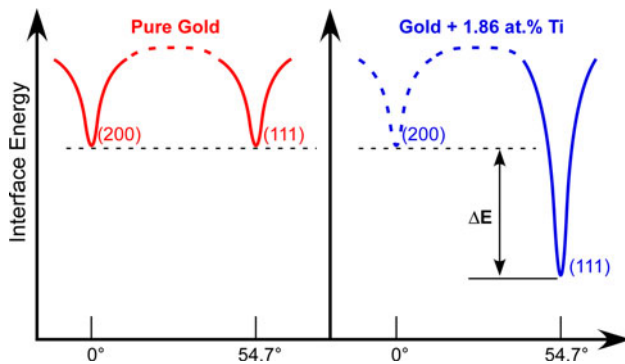


Fig. 7 Schematic drawing of the γ -plot for Au equilibrated in contact with the (0001) plane of sapphire. Ti segregation decreases the Au(111)–sapphire interface energy, resulting in the loss of low-index orientation relationships, the loss of the Au(200) preferred orientation, and only a Au(111) preferred orientation remains

at a single interface plane. Given the total amount of Ti measured at the interface and the thickness of the interface, it is likely that the interface film is composed of Al and oxygen, in addition to Ti. Unfortunately, the Al and oxygen content cannot be determined due to the presence of the adjacent sapphire substrate.

The formation of nanometer-thick intergranular films (IGF) at metal–alumina interfaces [61–66] and at grain boundaries in polycrystalline alumina [67, 68] has been characterized in the past, and described using DLVO theory [69, 70] and diffuse interface theory [71, 72]. Recently, using a model system similar to that used here, IGFs at Au–sapphire interfaces were shown to be an equilibrium effect where the presence of the IGF reduces the interface energy of the metal–ceramic interface, and image forces appear to be the dominant mechanism (rather than van der Waals forces) in reducing the interface energy [73]. Furthermore, the equilibrated IGF was described in terms of Gibbsian adsorption (segregation), where the conventional term describing the (chemical) excess was expanded to include order.

Here, the segregation of Ti, associated with a decrease in interface energy and the formation of a film at the nanometer thickness range, is most likely the same phenomena as IGFs (more recently called interface complexions [71–73]). As such, the Ti excess measured by quantitative EDS is only part of the excess term in the Gibbs adsorption isotherm, and a more complete structural analysis of the excess is required to fully thermodynamically describe the interface state. However, it is apparent from these results, that Ti segregation (without the formation of reaction products) can significantly reduce the interface energy, and may be an important component of improved wetting and spreading for so called reactive brazing systems.

Summary and conclusions

Model experiments designed to determine the influence of Ti segregation on the energy and structure of solid–solid Au–sapphire interfaces have been conducted using dewetted Au(Ti) films on (0001) sapphire. The advantage of this model configuration is that the relative energy, structure, and chemistry of the same interfaces can be determined. Chemical analysis using quantitative EDS shows a chemical Ti excess at the Au–sapphire interface of 2.2 Ti atoms/nm², which together with a chemical excess of 4.6 Ti atoms/nm² at the (0001) sapphire surface, is associated with a decrease in interface and surface energy. The segregated Ti at the Au–sapphire interface is distributed within a 1.54-nm thick intergranular film, which is not a bulk phase but rather an equilibrium interface state, which can change in thickness, chemistry, and structure as a function of thermodynamic parameters. Within the limits of the experimental conditions defined here, Ti segregation without the formation of a bulk reaction at the interface is associated with a decreased interface energy, and improved wetting. Thus, this may be an important part of the total complex mechanism responsible for improved wetting and spreading in “reactive” braze systems.

Acknowledgements The authors thank M. Katz for technical assistance, and D. Chatain, P. Wynblatt, and W.C. Carter for stimulating discussions. H.M. acknowledges support from the Women in Science program of the Israel Ministry of Science and an Ilan Ramon scholarship. This study was supported by the Israel Science Foundation (#163/05) and the Russell Berrie Nanotechnology Institute at the Technion.

References

- Zhou XB, De Hosson JTM (1996) *Acta Mater* 44(2):421
- Dezellus O, Eustathopoulos N (2010) *J Mater Sci* 45(16):4256. doi:10.1007/s10853-009-4128-x
- Loehman RE (1994) *Scr Metall Mater* 31(8):965
- Dalglish BJ, Saiz E, Tomsia AP, Cannon RM, Ritchie RO (1994) *Scr Metall Mater* 31(8):1109
- Levi G, Kaplan WD (2006) *J Mater Sci* 41(3):817. doi:10.1007/s10853-006-6565-0
- Saiz E, Tomsia AP (2005) *Curr Opin Solid State Mater Sci* 9(4–5):167
- Lipkin DM, Clarke DR, Evans AG (1998) *Acta Mater* 46(13):4835
- Nicholas MG, Mortimer DA (1985) *Mater Sci Technol* 1(9):657
- Gheta V, Chatain D (2002) *J Am Ceram Soc* 85(4):961
- Kapoor RR, Podszus ES, Eagar TW (1988) *Scr Metall* 22(8):1277
- Kritsalis P, Coudurier L, Eustathopoulos N (1991) *J Mater Sci* 26(12):3400. doi:10.1007/BF01124693
- Meier A, Chidambaram P, Edwards GR (1995) *J Mater Sci* 30(15):3791. doi:10.1007/BF01153936
- Gremillard L, Saiz E, Chevalier J, Tomsia AP (2004) *Z Metallkd* 95(4):261
- Howe JM (1993) *Int Mater Rev* 38(5):233

15. Akselsen OM (1992) *J Mater Sci* 27(8):1989. doi:[10.1007/BF01117909](https://doi.org/10.1007/BF01117909)
16. Frage N, Froumin N, Alzenshtein M, Kutsenko L, Fuks D, Dariel MP (2005) *Curr Opin Solid State Mater Sci* 9(4–5):189
17. Li JG (1992) *J Mater Sci Lett* 11(23):1551
18. Saiz E, Tomsia AP, Cannon RM (1998) *Acta Mater* 46(7):2349
19. Saiz E, Cannon RM, Tomsia AP (2000) *Adv Mater* 12(24):1952
20. Saiz E, Cannon RM, Tomsia AP (2000) *Acta Mater* 48(18–19):4449
21. Saiz E, Tomsia AP, Cannon RM (2001) *Scr Mater* 44(1):159
22. Cannon RM, Rühle M, Hoffmann MJ, French RH, Gu H, Tomsia AP, Saiz E (2000) Adsorption and Wetting Mechanisms at Ceramic Grain Boundaries, vol 118. Grain Boundary Engineering in Ceramics. The American Ceramic Society, Westerville, OH
23. Derby B, Holt S (2004) *Interface Sci* 12(1):29
24. Gremillard L, Saiz E, Radmilovic VR, Tomsia AP (2006) *J Mater Res* 21(12):3222
25. Eustathopoulos N (1998) *Acta Mater* 46(7):2319
26. Landry K, Eustathopoulos N (1996) *Acta Mater* 44(10):3923
27. Landry K, Rado C, Voitovich R, Eustathopoulos N (1997) *Acta Mater* 45(7):3079
28. Eustathopoulos N (2005) *Curr Opin Solid State Mater Sci* 9(4–5):152
29. Dezellus O, Hodaj F, Rado C, Barbier JN, Eustathopoulos N (2002) *Acta Mater* 50(5):979
30. Dezellus O, Hodaj F, Eustathopoulos N (2003) *J Eur Ceram Soc* 23(15):2797
31. Dezellus O, Hodaj F, Eustathopoulos N (2002) *Acta Mater* 50(19):4741
32. Muolo ML, Ferrera E, Morbelli L, Passerone A (2004) *Scr Mater* 50(3):325
33. Valenza F, Muolo ML, Passerone A (2010) *J Mater Sci* 45(8):2071. doi:[10.1007/s10853-009-3801-4](https://doi.org/10.1007/s10853-009-3801-4)
34. Voytovych R, Robaut F, Eustathopoulos N (2006) *Acta Mater* 54(8):2205
35. Mortensen A, Drevet B, Eustathopoulos N (1997) *Scr Mater* 36(6):645
36. Santella ML, Horton JA, Pak JJ (1990) *J Am Ceram Soc* 73(6):1785
37. Kozlova O, Voytovych R, Eustathopoulos N (2011) *Scr Mater* 65(1):13
38. Meltzman H, Chatain D, Avizemer D, Besmann TM, Kaplan WD (2011) *Acta Mater* 59(9):3473
39. Luo W, Jin Z, Liu H, Wang T (2001) *Calphad* 25(1):19
40. Chatain D, Chabert F, Ghetta V, Fouletier J (1993) *J Am Ceram Soc* 76(6):1568
41. Pilliar RM, Nutting J (1967) *Philos Mag* 16(139):181
42. Nichols FA, Mullins WW (1965) *Trans Metall Soc AIME* 233(10):1840
43. Wang Z, Wynblatt P (1998) *Surf Sci* 398(1–2):259
44. Sadan H, Kaplan WD (2006) *J Mater Sci* 41(16):5099. doi:[10.1007/s10853-006-0437-5](https://doi.org/10.1007/s10853-006-0437-5)
45. Thangadurai P, Lumelsky Y, Silverstein MS, Kaplan WD (2008) *Mater Charact* 59(11):1623
46. Baram M, Kaplan WD (2008) *J Microsc* 232(3):395
47. Thust A, Coene WMJ, Op de Beeck M, Van Dyck D (1996) *Ultramicroscopy* 64(1–4):211
48. Stadelmann PA (1987) *Ultramicroscopy* 21:131
49. Mobus G, Rühle M (1994) *Ultramicroscopy* 56(1–3):54
50. Alber U, Mullejans H, Rühle M (1997) *Ultramicroscopy* 69(2):105
51. Meltzman H, Kauffmann Y, Thangadurai P, Drozdov M, Baram M, Brandon D, Kaplan WD (2009) *J Microsc* 236(3):165
52. Fecht HJ, Gleiter H (1985) *Acta Metall* 33(4):557
53. Keast VJ, Williams DB (2000) *J Microsc* 199:45
54. Kumikov VK, Khokonov KB (1983) *J Appl Phys* 54(3):1346
55. Jia CL, Lentzen M, Urban K (2004) *Microsc Microanal* 10(2):174
56. Winterbottom WL (1967) *Acta Metall* 15(2):303
57. Herring C (1951) In: Kingston WE (ed) *The physics of powder metallurgy*. McGraw-Hill, New York, p 143
58. Hodgson BK, Mykura H (1973) *J Mater Sci* 8(4):565. doi:[10.1007/BF00550461](https://doi.org/10.1007/BF00550461)
59. Bonzel HP, Nowicki M (2004) *Phys Rev B* 70(24):1
60. Levi G, Kaplan WD (2003) *Acta Mater* 51(10):2793
61. McComb DW, Ning XG, Weatherly GC, Pan J, Lloyd DJ (2000) *Philos Mag A Phys Condens Matter Struct Defects Mech Prop* 80(11):2509
62. Scheu C, Dehm G, Kaplan WD (2001) *J Am Ceram Soc* 84(3):623
63. Avishai A, Scheu C, Kaplan WD (2003) *Z Metallkd* 94(3):272
64. Avishai A, Kaplan WD (2004) *Z Metallkd* 95(4):266
65. Avishai A, Scheu C, Kaplan WD (2005) *Acta Mater* 53(5):1559
66. Baram M, Kaplan WD (2006) *J Mater Sci* 41(23):7775. doi:[10.1007/s10853-006-0897-7](https://doi.org/10.1007/s10853-006-0897-7)
67. Brydson R, Chen S-C, Riley FL, Milne SJ, Pan X, Rühle M (1998) *J Am Ceram Soc* 81(2):369
68. Dillon SJ, Harmer MP (2007) *J Am Ceram Soc* 90(3):996
69. Clarke DR (1987) *J Am Ceram Soc* 70(1):15
70. Avishai A, Kaplan WD (2005) *Acta Mater* 53(5):1571
71. Tang M, Carter WC, Cannon RM (2006) *Phys Rev B* 73(2):024102
72. Tang M, Carter WC, Cannon RM (2006) *J Mater Sci* 41(23):7691. doi:[10.1007/s10853-006-0608-4](https://doi.org/10.1007/s10853-006-0608-4)
73. Baram M, Chatain D, Kaplan WD (2011) *Science* 332(6026):206